Journal of
MATERIALS RESEARCH

Welcome Comments Help

On the optimization of a dc arcjet diamond chemical vapor deposition reactor

S. W. Reeve[a] and W. A. Weimer
Chemistry Division, Naval Air Warfare Center, China Lake, California 93555

D. S. Dandy
Department of Chemical Engineering, Colorado State University, Fort Collins, Colorado 80523

(Received 14 June 1995; accepted 27 October 1995)

Based on results from chemical kinetic model calculations, a method to improve diamond film growth in a dc arcjet chemical vapor deposition reactor has been developed. Introducing the carbon source gas (CH_4) into an Ar/H_2 plasma in close proximity to the substrate produced diamond films exhibiting simultaneous improvements in quality and mass deposition rates. These improvements result from a reduced residence time of the methane in the plasma which inhibits the hydrocarbon chemistry in the gas from proceeding significantly beyond methyl radical production prior to encountering the substrate. Improvements in growth rate were modest, increasing by only a factor of two. Optical emission actinometry measurements indicate that the flux of atomic hydrogen across the stagnation layer to the substrate is mass diffusion limited. Since diamond growth depends upon the flux of atomic H to the substrate, these results suggest that under the conditions examined here, a low atomic H flux to the substrate poses an upper limit on the attainable diamond growth rate.

I. INTRODUCTION

Experimental measurements and chemical kinetic modeling results obtained previously in this laboratory have identified CH_3 as the dominant diamond growth precursor in our dc arcjet reactor.[1] Based on conclusions drawn from that work, an optimization strategy was developed to simultaneously improve the quality and growth rate of the diamond films produced in this reactor. The gas feed system was modified from introducing the gas feed into the plasma gun as a mixture (3% CH_4 in H_2), to one identical except that the CH_4 feed was injected into the plasma separately at a position midway between the gun and the substrate.[2] Herein we will refer to the former method as the *premixed* feed and the latter as the *remote CH_4* feed. The concept behind the remote CH_4 feed method was to limit the exposure time of the CH_4 to the hot plasma, thereby allowing sufficient time for CH_4 to react to produce CH_3 via $CH_4 + H \rightarrow CH_3 + H_2$ upstream of the substrate while forcing subsequent CH_3 consumption reactions to occur downstream of the substrate.[2] The goal was to determine the feasibility of increasing the CH_3 flux to the substrate while simultaneously reducing the flux of all other hydrocarbons by taking advantage of the high gas flow velocities produced in the reactor and the finite reaction kinetics of the hydrocarbon chemistry.[1–3] Diamond films grown using the remote CH_4 feed exhibited a significant enhancement in quality as evidenced by Raman spectra with reduced diamond peak linewidths.[2] However, while the quality of the diamond produced was improved, it was necessary to nearly double the CH_4 flow rate in order to achieve the same growth rate as the premixed gas feed, indicating a decrease in the efficiency with which the carbon in the feed was converted to diamond.[2,3] The decreased efficiency was due to the inability of the CH_4 to become radially well-mixed during the short transport time (~60 μs) from point of injection to the substrate.[2,3] Measurements of the carbon content of the gas at the substrate indicated that up to 66% of the injected carbon feed completely bypassed the substrate.[2]

In this work we present results obtained following an additional modification to the system designed to minimize the CH_4 feed gas exposure to the plasma by injecting the CH_4 at the substrate. We refer to this reactor feed method as *substrate CH_4 injection.* The extremely short exposure time of the CH_4 to the plasma maximizes the delivery of CH_4 and CH_3 to the substrate during deposition. As before, subsequent reactions involving CH_3 consumption will occur in the gas phase, though predominantly downstream of the substrate. Ideally, then, the only reactive hydrocarbon species encountering the substrate will be CH_3, as CH_4 is presumed to be unreactive. In addition, the close proximity of the CH_4 injection port outlet to the substrate is designed to address the low CH_4-to-diamond efficiency problem mentioned above.

[a]Current address: Department of Chemistry, Arkansas State University, State University, Arkansas 72467.

 © 1996 Materials Research Society

II. EXPERIMENTAL

The dc arcjet diamond reactor used in these experiments is a modified version of a system that has been previously described in detail.[1] During diamond deposition, only Ar was passed through the plasma gun electrode gap, creating a high velocity plasma that impinged at normal incidence onto a water-cooled molybdenum substrate positioned 2.5 cm from the gun outlet. In the present configuration, the H_2 and CH_4 were introduced into the reactor through separate feed lines, as shown in Fig. 1. H_2 was injected into the Ar plasma as before, 1 cm downstream of the electrode gap through opposing side ports integral to the plasma gun, while CH_4 was injected 3.5 cm downstream of the H_2 ports through a stainless steel tube mounted onto the substrate holder, as shown in Fig. 1. Typical reactor operating parameters are given in Table I.

Using the substrate CH_4 injection arrangement, a series of diamond films was grown under varied deposition conditions. Mass deposition rates were determined by substrate weight difference. The films produced were characterized using Raman spectroscopy and optical microscopy. Films were grown for 20–30 min to ensure the formation of crystallites large enough to be examined by optical microscopy. Raman spectra were collected using an Ar^+ laser (488 nm, 75 mW) with an incident beam diameter of 60 μm. To assess the relative quality of each film, the full width at half maximum (FWHM) of the diamond peak was determined by performing a least squares fit of the Raman spectra using a fitting function consisting of a single Lorentzian peak superimposed upon a quadratic background.[4-7]

Stable reactor exhaust gas component concentrations were determined using a UTI Model 100C quadrupole mass spectrometer interfaced with a LeCroy Model 9400

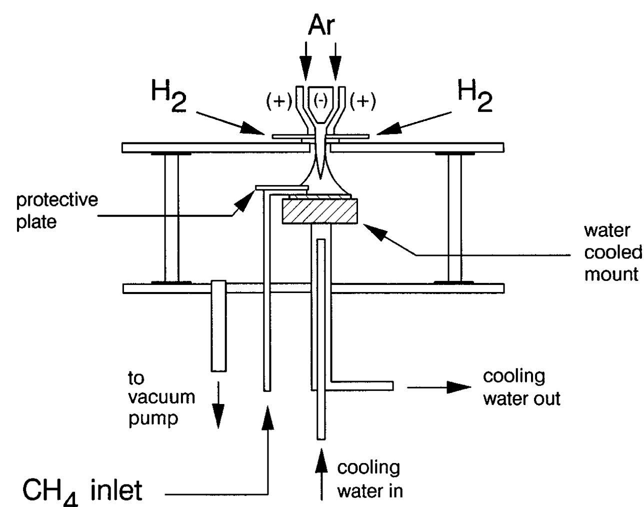

FIG. 1. Schematic diagram of the dc arcjet diamond reactor incorporating the substrate CH_4 injection system.

TABLE I. Nominal dc arcjet CVD reactor operating parameters.

Parameter	Value
Dc voltage	20 V
Dc current	140–150 A
Reactor pressure	55–60 Torr
Substrate	Molybdenum (25 mm × 38 mm)
Plasma gun–substrate distance	~2.5 cm (~1 inch)
Ar flow rate	13.7 slm
H_2 flow rate	5.4 slm
CH_4 flow rate	150–700 sccm

digital oscilloscope and a Hewlett-Packard Model 9836 computer via an IEEE-488 bus. The mass spectrometer response was calibrated by sampling the reactor exhaust following addition of known amounts of CH_4, C_2H_2, C_2H_4, C_2H_6, CO and CO_2 to fixed reactor feed flows of H_2 (5.4 slm) and Ar (13.7 slm) with the plasma turned off. Experimentally determined hydrocarbon cracking patterns were found to be necessary to account for complications that occur when high hydrogen partial pressures exist in the ion source region of mass spectrometers utilizing electron impact ionization.[8,9] Electrode surfaces are bombarded with atomic hydrogen created on the hot filament in the ionizer, generating significant background levels of H_2O, CO_x, and C_mH_n.[8,9] The presence of these background species alters the observed hydrocarbon cracking patterns from typical literature values. The observed height of each peak P_j in the mass spectrum is the sum of contributions from the various hydrocarbon species detected. Thus, a fitting function was constructed to fit all peak heights in the mass spectrum simultaneously, where $P_j = \sum F_i[C_i]$, where P_j is the height of mass spectral peak j, F_i is the fractional contribution of species i to the peak, and $[C_i]$ is the concentration of species i.[1] The summation is performed for all species producing signals between 5 amu and 55 amu. Only the C_i values are varied during the fit to determine the hydrocarbon concentrations.

Optical emission spectra for actinometry analyses were obtained by imaging the luminous plasma emission onto the end of a 1.0 mm diameter fiber optic bundle with a 200 mm focal length biconvex quartz lens. A Tracor Northern Model TN6500 optical multichannel analyzer (OMA) equipped with an intensified 1024 element photodiode array detector, 0.5 nm bandpass, was used to record the emission spectra. The OMA was calibrated for spectral response using an Optronics Laboratories Model 220M standard tungsten lamp.

III. RESULTS AND DISCUSSION

In Fig. 2, the mass deposition rates for films grown using the substrate CH_4 injection scheme are shown along with results for films grown using the remote CH_4 and premixed gas feeds. These films were grown while varying the CH_4 gas feed flow rate; the Ar and H_2

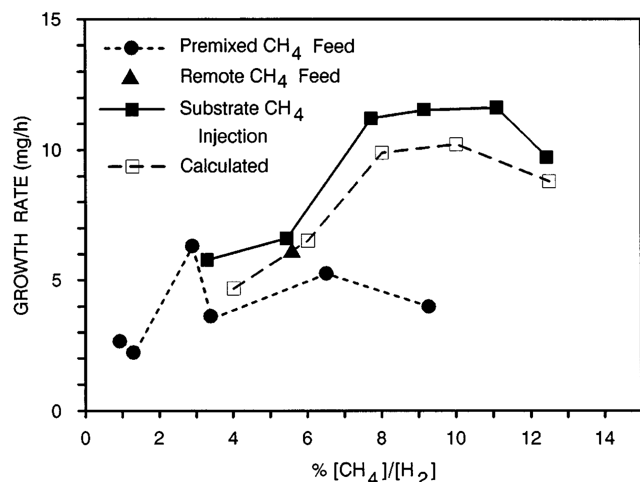

FIG. 2. Measured diamond mass deposition rates versus CH_4/H_2 percentage in reactor feed gas for various CH_4 gas feed methods. Calculated deposition rates are for the substrate CH_4 injection method. Feed gas flow rates for Ar and H_2 were held constant at 13.7 slm and 5.4 slm, respectively.

flow rates were held constant at 13.7 slm and 5.4 slm, respectively. Deposition rates for films grown using the premixed feed are limited to lower CH_4/H_2 feed ratios, since ratios greater than ~3% produced black films for which the Raman spectra indicated the presence of significant amounts of non-diamond carbon. Similar results were obtained using the remote CH_4 feed for CH_4/H_2 ratios greater than 6%. With the substrate methane injection design, high quality diamond films have been produced with CH_4/H_2 feed ratios as high as 12%. Although the mass deposition rate increased by a factor of 2 at the higher CH_4 flows, there appears to be little advantage in using a CH_4/H_2 feed ratio above about 8%.

Calculated diamond deposition rates for the substrate CH_4 injection method, also shown in Fig. 2, agree extremely well with measured values. The calculated results were obtained using a boundary-layer model (CRESLAF),[10] coupled with a simplified surface kinetics mechanism given in Table II.[11] For the reactions (1)–(3) in the text below and those listed in Table II, CH(s) denotes a hydrogenated surface carbon, C*(s) denotes a surface carbon radical, CM(s) denotes a methylated surface carbon, and CM*(s) denotes a CH_2 radical bound to a surface carbon. The model predicts that injecting the CH_4 inside the boundary layer, close to the substrate, proves to be beneficial for two reasons. First, the residence time of the hydrocarbon in the hot gas mixture is very short, and the gas-phase chemistry does not have sufficient time to proceed significantly past the reaction:

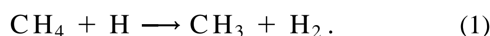

$$CH_4 + H \longrightarrow CH_3 + H_2 . \qquad (1)$$

Subsequent hydrogen abstraction reactions do occur, but only small concentrations of CH_x $(x = 0, 1, 2)$ are predicted to form within the boundary layer. Further, small concentrations of atomic carbon through methylene radical species and short residence times lead to relatively small conversion of the C1 species to C2 species. A series of boundary-layer calculations carried out in this system predict that, at the outer edge of the substrate where $[C_2H_2]$ is maximum, $[CH_3]$ is larger by a factor of up to five, even though CH_3 is being depleted by deposition downstream of the injector (brackets denote concentration). These relative concentrations of CH_3 and C_2H_2 are in marked contrast to those observed near the substrate under premixed conditions; in that system, $[C_2H_2]$ can be between 10 and 30 times greater than $[CH_3]$ adjacent to the substrate. The second benefit of injecting the hydrocarbon within the boundary layer is that, by definition, all reactive species formed have a finite probability of reacting with the surface. No activated species can be "blown by" the substrate without possibility of contact.

The enhancement of growth rate through substrate injection is directly proportional to the amount of atomic hydrogen present inside the boundary layer. At the pressure considered in this study, 55 Torr, the system is

TABLE II. Surface chemistry mechanism used in boundary-layer calculations.[a] Reaction rate coefficient $= A^b e^{-(E/RT)}$.

Reaction[b]	A	b	E
CH(s) + H → C*(s) + H_2	6.19×10^{13}	0	7300
C*(s) + H → CH(s)	1.70×10^{13}	0	0
C*(s) + CH_3 → CM(s)	3.30×10^{12}	0	0
CM(s) → C*(s) + CH_3	1.29×10^{15}	0	61000
CM(s) + H → CM*(s) + H_2	4.27×10^{13}	0	7300
CM*(s) + H → CH(s) + H_2 + diamond	8.54×10^{14}	0	7300
C*(s) + C → C*(s) + diamond	3.30×10^{12}	0	0
CM*(s) + CH_3 → CM(s) + defect + H_2	7.50×10^{8}	0	0
CM*(s) + C → C*(s) + defect + diamond + H_2	7.50×10^{8}	0	0

[a]From Ref. 11.
[b]Species symbols defined in text.

mass-transfer limited in atomic hydrogen. This limitation manifests itself as a dramatic drop in [H] from its free stream value to that at the surface. The two surface reactions responsible for this drop in H across the boundary layer are

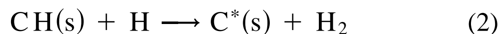

$$CH(s) + H \longrightarrow C^*(s) + H_2 \qquad (2)$$

and

$$C^*(s) + H \longrightarrow CH(s). \qquad (3)$$

The mole fraction of H at the surface X_H^s is related to the free stream value X_H by simple transport theory:[11]

$$\frac{X_H^s}{X_H} = \frac{2k_2k_3\Gamma\delta}{(k_2 + k_3)D_H} = \frac{1}{1 + Da}, \qquad (4)$$

where k_2 and k_3 are the rate constants for Eqs. (2) and (3), Γ is the total concentration of surface sites, D_H is the diffusivity of H in Ar, and Da is the effective Damköhler number, which is the ratio of the rate of destruction of H by surface reactions to the rate of transport of H through the boundary layer to the surface by diffusion. The boundary-layer thickness, δ, is given by

$$\delta \approx 2\sqrt{\frac{LD_H}{U_\infty}}, \qquad (5)$$

where L is the torch-to-substrate distance and U_∞ is the average velocity of the gas exiting the plasma gun. For this arcjet system, it is estimated from Eq. (4) that $X_H^s/X_H \approx 0.06$. This prediction is borne out by experimental observation. Since only 1% of the injected H_2 into the plasma gun dissociates to form H,[1] the amount of H present inside the boundary layer reacting with the injected CH_4 comprises only about 0.2% of the total gas mixture.

Both measured and calculated deposition rates in Fig. 2 exhibit identical functionality (initial increase, plateau, and then fall off) with increasing CH_4 percentages in the rector gas feed. At relatively low CH_4/H_2 feed ratios, the increase in growth rate is due to an increase in the concentration of activated carbon (predominantly CH_3) in the gas phase near the substrate via reaction (1). At higher CH_4/H_2 ratios, the deposition rate levels off because reaction (1) competes with reaction (2) for available gas phase H, effectively limiting the rate at which reactive sites are formed on the surface via reaction (2). At very high CH_4/H_2 ratios, the deposition rate falls as reaction (1) depletes the gas phase of H, which reduces the rate of reactive site formation, reaction (2).

Spatially resolved Raman spectra for a representative film grown using the substrate CH_4 injection method are shown in Fig. 3. The absence of a significant non-diamond feature in the spectra indicates that the reported mass deposition rates are attributable largely to diamond, although in peripheral regions of the film, there is some evidence in the spectra of a non-diamond carbon phase. Also, the films grown with substrate injection are nearly white in color, as opposed to the characteristic off-white/gray color of the films produced using the premixed and remote CH_4 gas feeds. This coloration is due to an accumulation of amorphous and/or graphitic carbon in the films, presumably at the grain boundaries.

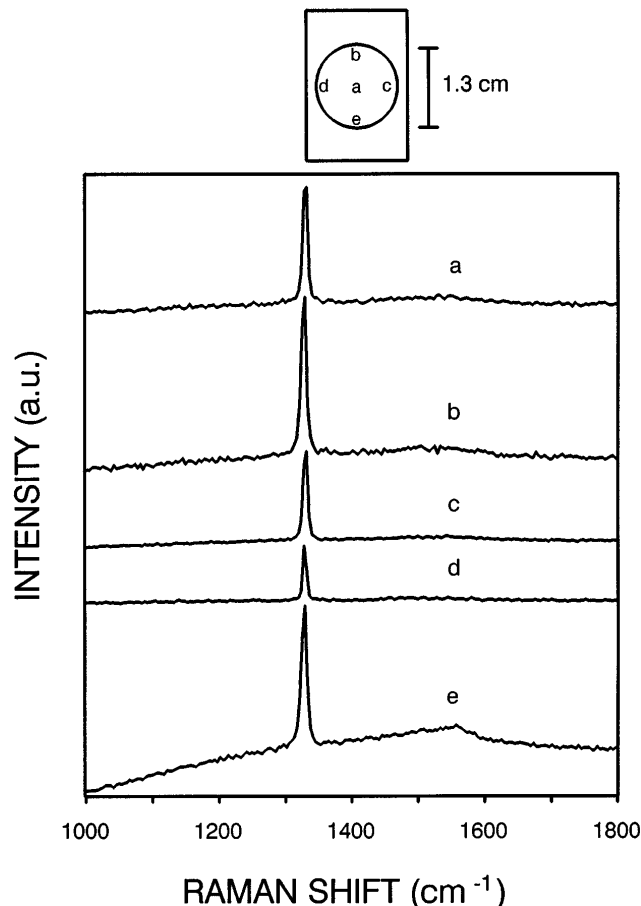

FIG. 3. Spatially resolved Raman spectra for a diamond film grown using the substrate CH_4 injection method. Spectra labeled a–e correspond to positions a–e indicated in diagram of a 1.3 cm diameter circular diamond film on a rectangular Mo substrate.

Raman spectroscopic measurements provide an assessment of diamond quality that is largely qualitative and interpretation of spectra is subject to a number of difficulties. Although the scattering efficiency of graphite is about 50 times that of diamond in the visible,[12,13] graphite is strongly absorbing (optical absorption coefficient $\alpha = 3.4 \times 10^5$ cm^{-1})[14] while diamond is transparent. Consequently, the sp^2 bonded carbon in the film is capable of absorbing a significant portion of both the incoming laser and the outgoing Raman scattered radiation.[15] A CVD diamond film containing a small amount of a non-diamond carbon would be expected, therefore, to exhibit a Raman spectrum with fewer detected scattered photon counts, but not

necessarily a discernible non-diamond carbon peak. The top trace in Fig. 4 is a Raman spectrum obtained from a white diamond film produced with the substrate CH_4 injection reactor design, while the lower two spectra are from the highest quality diamond films we have grown with the remote CH_4 (off-white) and premixed (gray) gas feeds. Features due to non-diamond carbon are absent in all three spectra. What is strikingly evident, however, is the reduced number of photon counts measured for the light gray films produced using the remote CH_4 and premixed gas feeds. We ascribe the decreased Raman spectral intensities of these films as due to absorption by non-diamond carbon.

The existence of impurities and/or crystal defects in diamond also affects the line shapes of the Raman spectral features.[4–7,12] Relatively high quality diamond films are characterized by Raman spectra lacking the broad band due to sp^2 bonded carbon at about 1560 cm^{-1}. For these films, semiquantitative assessments of quality are performed by comparing the linewidth of the diamond peak at 1332 cm^{-1} to the benchmark value of 2.0 cm^{-1} for gem quality single crystal diamond.[4,12] We have found that our films may produce FWHM linewidths at 1332 cm^{-1} as high as 13 cm^{-1} with no discernible non-diamond feature. The Raman FWHM linewidths of the 1332 cm^{-1} diamond peak for the films represented in Fig. 4 are 10.9 cm^{-1} for the film using the premixed feed, 4.5 cm^{-1} for the film grown using the remote methane feed, and 4.2 cm^{-1} for the film grown using substrate methane injection. An obvious improvement in the quality of the films is observed using the remote CH_4 feed and/or the substrate CH_4 injection, compared to the premixed feed. FWHM linewidths for films grown using the substrate CH_4 injection method while varying the CH_4 feed flow rate are shown in Fig. 5. For comparison, the linewidths for the highest quality films produced using the premixed and remote feed methods (no non-diamond feature in the Raman spectra) are included in Fig. 5. Unusually high CH_4/H_2 feed gas percentages, up to 12%, may be used with the substrate CH_4 injection to produce high quality films, whereas most other diamond CVD systems produce non-diamond films above a CH_4/H_2 feed gas percentage of 0.5–2%.[16] Diamond is produced in this system at high CH_4/H_2 feed gas ratios largely because the residence time of the CH_4 in the plasma is extremely short, allowing only CH_4, which cannot bind as-is to the diamond surface, and CH_3, which is an effective diamond precursor, to encounter the substrate surface. Other hydrocarbons are, in fact, formed in the reactor, although predominantly downstream of the substrate where they do not participate in film formation.

A noteworthy observation made during the course of this study is that both the remote CH_4 and substrate CH_4 injection gas feed methods produced high quality, small-grained films. The Raman spectra shown in Fig. 4 represent films (of equal deposition times) with grain sizes of 0.5–2 μm, 1.2–2.4 μm, and 6–7.2 μm for the substrate CH_4 injection, remote CH_4, and premixed feed methods, respectively. Only relatively large-grained films produced Raman spectra with no non-diamond carbon feature using the premixed feed, whereas small-grained films produced with this gas feed method were darker and noticeably of inferior quality. The ability to produce high quality, small-grained films is of value for applications requiring thin films of high strength, since polycrystalline materials generally show an inverse relationship between strength and the square root of grain size.[17]

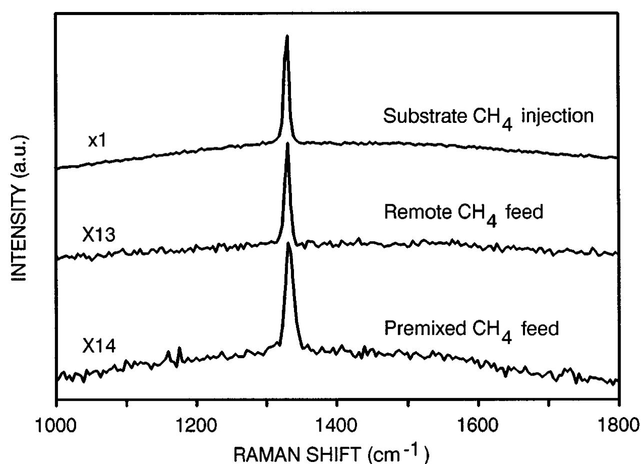

FIG. 4. Raman spectra of diamond films grown using various gas feed methods. The substrate CH_4 method produces films exhibiting the most intense Raman spectra with the narrowest diamond linewidth at 1332 cm^{-1}.

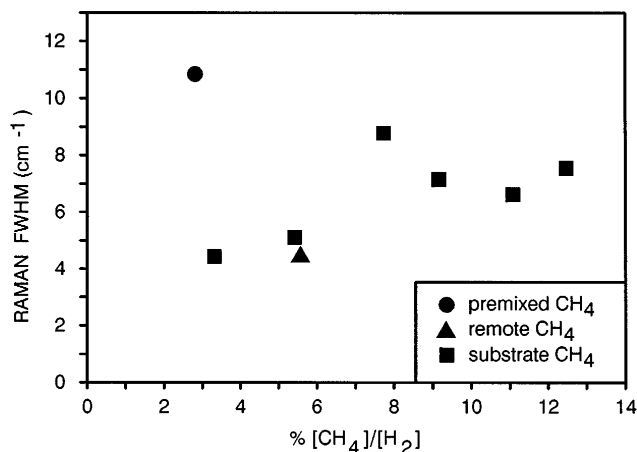

FIG. 5. Full width at half maximum (FWHM) linewidths of the diamond peak at 1332 cm^{-1} in Raman spectra of films grown using varying CH_4/H_2 percentages in the reactor feed gas for various CH_4 feed gas methods. Feed gas flow rates for Ar and H_2 were held constant at 13.7 slm and 5.4 slm, respectively.

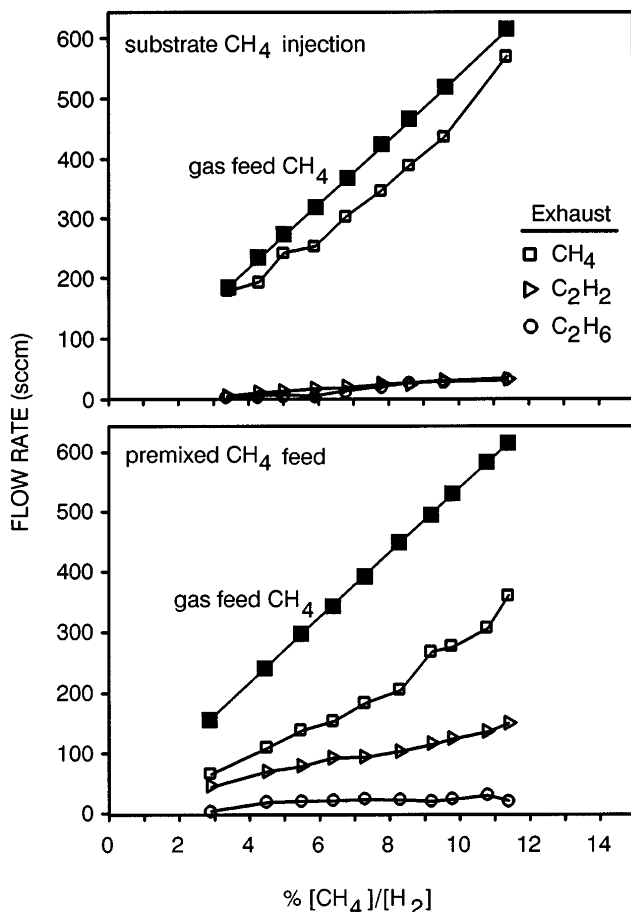

FIG. 6. Reactor exhaust component gas flow rates detected by mass spectrometry versus CH_4/H_2 percentage in reactor feed gas for substrate CH_4 injection and premixed CH_4 feed methods. Feed gas flow rates for Ar and H_2 were held constant at 13.7 slm and 5.4 slm, respectively, while the feed gas CH_4 flow rate (large solid squares) was varied between 154 sccm and 615 sccm.

The chemical effect of the reduced CH_4 residence time in the plasma is indicated in Fig. 6, which shows the reactor exhaust gas composition determined by mass spectrometry as a function of the CH_4/H_2 feed gas percentage. Note that the Ar and H_2 feed gas flow rates were held constant at 13.7 slm and 5.4 slm, respectively. It is clear in Fig. 6 that although identical exhaust gas components are detected (CH_4, C_2H_2, and C_2H_6), a larger percentage of the feed gas CH_4 passes through the reactor intact for the substrate CH_4 injection feed system as compared to the premixed feed system.

The data in Fig. 7 were collected under identical conditions except that the gas was sampled at the substrate. The sampling port inlet was located at the opposite end of the substrate relative to the gas feed port to sample gas that had been injected and traversed the substrate, a distance of about 1 cm. The data in Fig. 7 show that although the amount of C_2H_2 and C_2H_6 detected relative to CH_4 is greater than for the exhaust gas

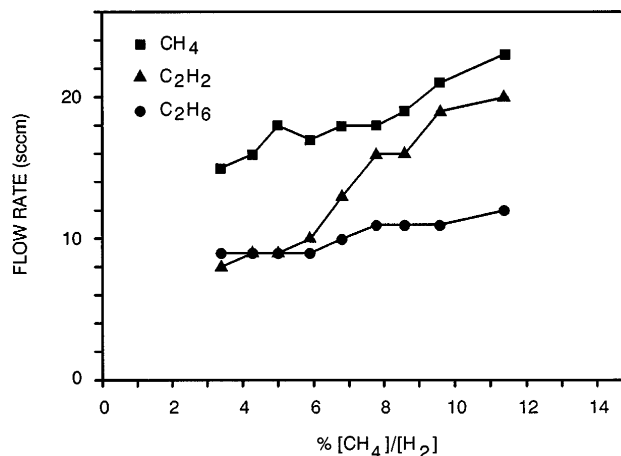

FIG. 7. Stable component gas flow rates detected by mass spectrometry while sampling at the substrate versus CH_4/H_2 percentage in reactor feed gas for the substrate CH_4 injection feed gas method. Feed gas flow rates for Ar and H_2 were held constant at 13.7 slm and 5.4 slm, respectively, while the feed gas CH_4 flow rate was varied between 183 sccm and 615 sccm.

measurements, the amount of carbon detected (in the form of CH_4, C_2H_2, and C_2H_6) is only about 14–27% of that injected as CH_4. This is in contrast with the exhaust gas measurements in Fig. 6 where, within experimental error, 100% of the carbon injected as CH_4 is detected as CH_4, C_2H_2, and C_2H_6. The low percentage of total detected carbon reveals that most of the carbon injected at the substrate never reaches the mass spectrometer sampling port and, thus, does not mix completely with the plasma. Although injecting the CH_4 in the boundary layer ensures that all of the injected carbon contacts the substrate, most of the carbon source gas flows through the reactor without binding to the substrate, resulting in a low gas phase carbon-to-diamond conversion efficiency. Of the gas that is sampled at the substrate, most of the carbon is in the form of C_2H_2, which indicates that the residence time in the boundary layer is sufficient for appreciable feed gas activation near the substrate. These results are similar to those we reported using the remote CH_4 gas feed[2] where only 36% of the carbon injected as CH_4 was detected at the substrate as CH_4, C_2H_2, and C_2H_6. It appears, then, that in order to reduce the carbon source gas residence time to enhance the delivery of CH_3 to the substrate, the gas feed carbon-to-diamond conversion efficiency is substantially reduced as well.

The low carbon-to-diamond conversion efficiency is dictated by the concentration of atomic H in the boundary layer, which drives the rates of both radical site creation on the diamond surface [Eq. (2)] and CH_4-to-CH_3 conversion [Eq. (1)]. Dandy and Coltrin[18] have reported model results indicating that the atomic H concentration in the boundary layer is 2 to 10 times lower than that for the free stream region of the plasma.

Therefore, an attempt to examine the atomic H concentration in the system was undertaken. In Ref. 19, spatially resolved optical emission spectra collected from this system were reported, indicating the presence of a boundary layer up to ~9 mm thick above the substrate under diamond growth conditions. Within the boundary layer, the optical emission intensity for both atomic hydrogen and argon increased significantly. Because the emission line intensities can vary with changing plasma conditions, their use to determine relative changes in ground state species concentration is not reliable.[20] In some cases, however, the technique of actinometry has been successfully applied to correct for variations in plasma conditions.[20–26] In actinometry, the ratio of the optical emission intensities of the species of interest (emitter) and that of an inert species (actinometer) is evaluated to determine relative changes in the ground state concentration of the emitter. The validity of actinometry rests upon the assumption that changes in plasma conditions will affect the emission intensities of the emitter and actinometer similarly. Results obtained by actinometry have been verified for a number of plasma systems by comparison to ground state concentration measurements obtained with laser induced fluorescence.[27–31] Since both atomic hydrogen and argon are strong emitters in our system, actinometry would appear to be applicable as a means to examine ground state hydrogen atom concentrations despite large fluctuations in plasma parameters such as electron energy distribution and density.

Of interest here is the ground state concentration for atomic hydrogen. This is obtained through the relation $I_H/I_{Ar} = K([H]/[Ar])$, where I_H and I_{Ar} are the optical emission intensities of H and Ar, respectively, K is a proportionality constant, [H] is the ground state concentration of the atomic hydrogen, and [Ar] is the ground state concentration of argon.[27] In order to substantiate the validity of using actinometry to determine the H concentration profile in our reactor, a series of optical emission measurements was made using the premixed feed method with the substrate lowered to the bottom of the reactor vessel, far from the plasma gun outlet. The plasma, therefore, was essentially freeflowing, much like a premixed flame. This arrangement allowed the direct application of the Sandia PREMIX[32,33] flame code to model the plasma, since we had previously demonstrated the validity of the model for our reactor.[1] The experimental [H] profile is obtained by plotting the ratio of the $H\alpha$ optical emission intensity at 656 nm (I_H) to the optical emission intensity of the argon line at 696 nm (I_{Ar}) as a function of reactor axial distance. A comparison of the calculated atomic H plasma centerline profile with the actinometric measurements versus distance from the plasma gun is shown in Fig, 8. The experimental H atom concentration profile, represented by the data points in

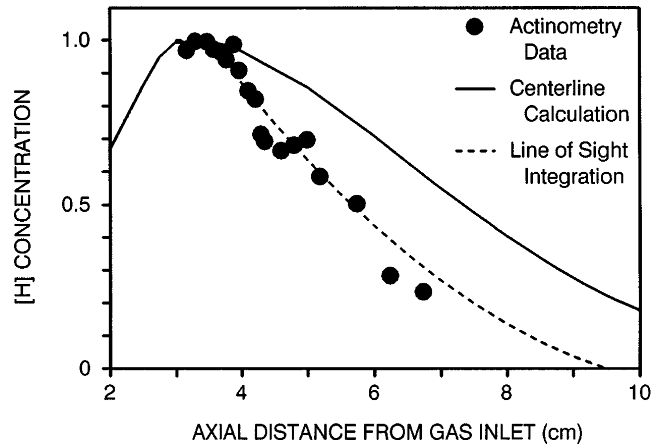

FIG. 8. Atomic H concentration profiles, normalized to maximum values of 1, determined by actinometry, PREMIX centerline calculations, and line-of-sight integration.

Fig. 8, appears to decrease faster with axial distance than the calculated [H] centerline concentration. This discrepancy is not surprising, since the model calculates concentration profiles along the centerline of the plasma and the actinometry optical emission is collected from all points along a line-of-sight that is orthogonal to the plasma centerline.

The luminous glow of the plasma jet takes on a well-defined conical shape, expanding from a radius $r = 0.5$ cm when confined to the bore of the plasma gun to $r = 1.75$ cm approximately 2.54 cm downstream of the plasma gun.[1] To relate the calculated centerline [H] profile to the profile obtained using the actinometric intensity ratio experiment, we make the following assumption: there exist in the plasma jet axisymmetric hemispherical contours of equal atomic H concentration defined by vectors of equal length emanating from a single point of origin (here, the feed gas inlet at the plasma centerline). A schematic diagram illustrating this assumption is shown in Fig. 9(a). Implicit in the assumption is that the centerline calculation establishes a concentration versus distance relationship that is valid along any of these vectors. The line-of-sight optical emission measurement is necessarily sampling the concentration across the hemispherical contours along a line as shown in Fig. 9(a). In an emission measurement taken at a given axial position, in addition to the signal produced at the centerline, there will be contributions to the signal along the line-of-sight that correspond to longer distances [longer vectors in Fig. 9(a)] from the origin. These positions are equivalent to positions along the centerline at distances downstream of the measurement position. To account for the line-of-sight effect, the actinometric measurement (I_H/I_{Ar}) is related to the

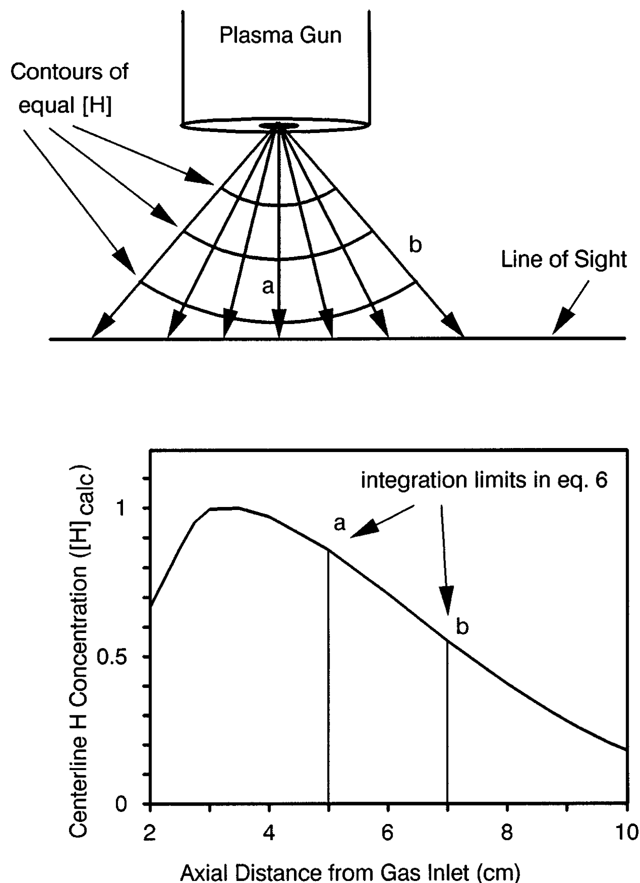

FIG. 9. Schematic diagram illustrating line-of-sight optical emission integration method using the CHEMKIN/PREMIX centerline atomic H (H_{calc}) calculations.

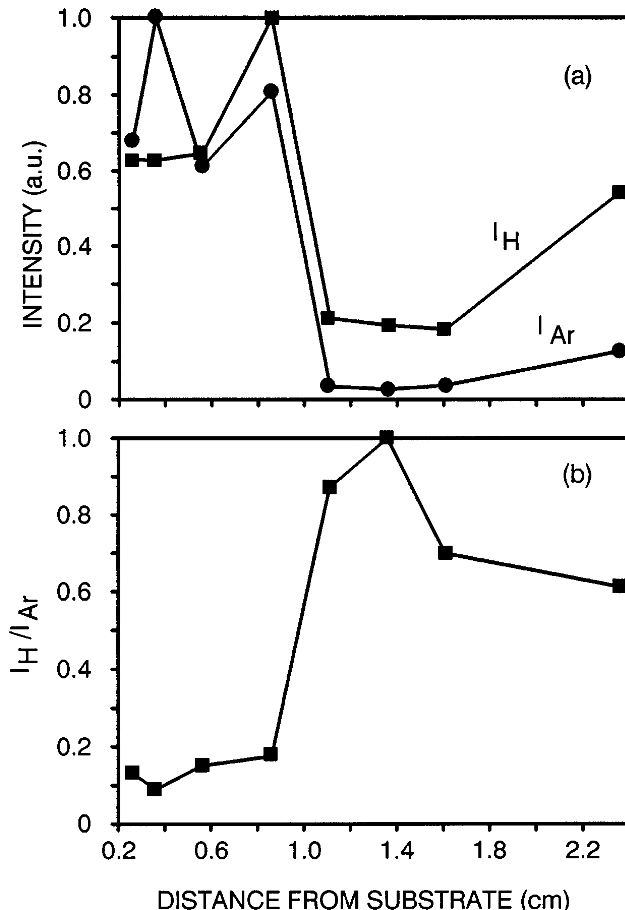

FIG. 10. Profiles of (a) optical emission intensities for H (656 nm) and Ar (696 nm) and (b) atomic H determined by actinometry using data in (a).

calculated atomic hydrogen concentration $[H]_{calc}$ by:

$$\frac{I_H}{I_{Ar}} \propto 2 \int_a^b [H]_{calc}\, dx\,, \tag{6}$$

where the factor 2 accounts for integration across the entire plasma diameter, x is the distance along the plasma centerline, a is the centerline distance of the line-of-sight, and b is the distance from the origin to the line-of-sight along the outermost vector, as illustrated in Fig. 9. The integration is performed numerically over $[H]_{calc}$, as shown in Fig. 9. This line-of-sight correction produces an integrated [H] concentration profile that is in agreement with the experimental observation, as shown in Fig. 8. The observed agreement provides a level of confidence in the actinometric measurements taken with the substrate in place.

Concentration profiles determined by actinometry for atomic H with the substrate in place are shown in Fig. 10. The profile in Fig. 10 indicates that [H] rises to a maximum at a point ~1.3 cm above the substrate, falls rapidly over a distance of ~2 mm, and then levels off for the remaining distance to the substrate. The significance of Fig. 10 is that the amount of atomic H that reaches the diamond growth surface is severely mass diffusion limited under these reactor conditions and, consequently, there is an upper limit on the attainable rate of diamond film growth possible for these reactor conditions.

IV. CONCLUSIONS

Results presented here are consistent with the hypothesis that CH_3 is the primary gas-phase diamond growth precursor. The role of atomic H in diamond synthesis has been relatively well established: (1) production of reactive hydrocarbons in the gas phase, (2) creation of radical sites on the diamond surface, and (3) stabilization of sp^3 bonding for carbon species bound to the diamond surface. It appears, then, that for systems producing relatively low levels of atomic H, such as ours, a method of inhibiting the hydrocarbon chemistry beyond CH_3 production is advantageous and should be considered in reactor design. We cannot rule out the possibility that the other species formed (CH_2, CH, and C) contribute to diamond growth to some minor extent,

although measures taken to avoid their presence at the substrate appear to be beneficial.

We regard the diamond deposition rates observed here to be low. Operating at lower pressures would ease the mass-transfer limitation that the system is operating under, and would, in theory, increase the diamond deposition rate. The growth rate levels and the dependence upon gas feed CH_4/H_2 ratios illustrated in Fig. 2 are due primarily to the small concentration of H in the gas phase at the substrate, which is limited by the low amount ($\sim$1%) of feed gas H_2 dissociated in the reactor and a dramatic drop in atomic H concentration across the boundary layer.

ACKNOWLEDGMENTS

This work was supported in part by the Office of Naval Research. S.W.R. acknowledges the Office of Naval Research and the American Society for Engineering Education for a Postdoctoral Fellowship. D.S.D. wishes to acknowledge the support of the Materials Science Program at ARPA, Contract N00014-93-1-2002.

REFERENCES

1. S.W. Reeve, W.A. Weimer, and F.M. Cerio, J. Appl. Phys. **74**, 7521 (1993).
2. S.W. Reeve, W.A. Weimer, and D.S. Dandy, Appl. Phys. Lett. **63**, 2487 (1993).
3. S.W. Reeve and W.A. Weimer, Thin Solid Films **253**, 103 (1994).
4. J.W. Ager III, D.K. Veirs, and G.M. Rosenblatt, Phys. Rev. B **43**, 6491 (1991).
5. L.H. Robins, E.N. Farabaugh, and A. Feldman, J. Mater. Res. **5**, 2456 (1990)
6. M. Yoshikawa, H. Ishida, A. Ishitani, S. Koizumi, and T. Inuzuka, Appl. Phys. Lett. **58**, 1387 (1991).
7. S.C. Sharma, M. Green, R.C. Hyer, C.A. Dark, T.D. Black, A.R. Chourasia, D.R. Chopra, and K.K. Mishra, J. Mater. Res. **5**, 2424 (1990).
8. H.F. Dylla and W.R. Blanchard, J. Vac. Sci. Technol. A **1**, 1297 (1983).
9. G.A. Rozgonyi, J. Vac. Sci. Technol. **3**, 187 (1983).
10. M.E. Coltrin, H.K. Moffat, R.J. Kee, and F.M. Rupley, Sandia Report SAND93-0478 (1993).
11. D.S. Dandy and M.E. Coltrin, J. Mater. Res. **10**, 1993 (1995).
12. D.S. Knight and W.B. White, J. Mater. Res. **4**, 385 (1989).
13. N. Wada, P.J. Gaczi, and S.A. Solin, J. Non-Cryst. Solids **35/36**, 543 (1980).
14. A. Borghesi and G. Guizzetti, in *Handbook of Optical Constants of Solids,* edited by E.D. Palik (Academic Press, New York, 1991), p. 458. Absorption coefficient $\alpha = 4\pi k/\lambda$, using $k = 1.31$ and $\lambda = 488.0$ nm.
15. R.E. Shroder, R.J. Nemanich, and J.T. Glass, Phys. Rev. **41**, 3738 (1990).
16. T.D. Moustakas, in *Synthetic Diamond: Emerging CVD Science and Technology,* edited by K.E. Spear and J.P. Dismukes (Wiley, New York, 1994), Chap. 6.
17. D.C. Harris, *Infrared Window and Dome Materials* (SPIE Optical Engineering Press, Bellingham, WA, 1992), pp. 69, 70.
18. D.S. Dandy and M.E. Coltrin, Appl. Phys. Lett. **66**, 391 (1995).
19. S.W. Reeve and W.A. Weimer, Thin Solid Films **236**, 91 (1993).
20. F.G. Celii and J.E. Butler, Ann. Rev. Phys. Chem. **42**, 643 (1991).
21. J.W. Coburn and M. Chen, J. Appl. Phys. **51**, 3134 (1980).
22. R.A. Gottscho and T.A. Miller, Pure & Appl. Chem. **56**, 189 (1984).
23. R.W. Dreyfus, J.M. Jasinski, R.E. Walkup, and G.S. Selwyn, Pure & Appl. Chem. **57**, 1265 (1985).
24. T.A. Miller, J. Vac. Sci. Technol. A **4**, 1768 (1986).
25. J.A. Mucha, D.F. Flamm, and D.E. Ibbotson, J. Appl. Phys. **65**, 3448 (1989).
26. W. Zhu, A. Inspektor, A.R. Badzian, T. Mckenna, and R. Messier, J. Appl. Phys. **68**, 1489 (1990).
27. A. Granier, D. Chereau, K. Henda, R. Safari, and P. Leprince, J. Appl. Phys. **75**, 104 (1994).
28. R. d'Agnostino, F. Cramarossa, S. De Benedictis, and G. Ferraro, J. Appl. Phys. **52**, 1259 (1981).
29. R.A. Gottscho, G.P. Davis, and R.H. Burton, J. Vac. Sci. Technol. A **1**, 622 (1983).
30. R.A. Gottscho and V.M. Donnelly, J. Appl. Phys. **56**, 245 (1984).
31. R.E. Walkup, K.L. Saenger, and G.S. Selwyn, J. Chem. Phys. **84**, 2668 (1986).
32. R.J. Kee, F.M. Rupley, and J.A. Miller, Sandia National Laboratories Report, SAND89-8009 (1989).
33. R.J. Kee, J.F. Grcar, M.D. Smooke, and J.A. Miller, Sandia National Laboratories Report, SAND85-8240 (1985).